NUCL SCI TECH (2018) 29:167
https://doi.org/10.1007/s41365-018-0495-9

Investigation of the radiosensitization effect in FePt nanopaticle clusters with Monte Carlo simulation

Peng-Yuan Qi[1] · Zhi-Tao Dai[1] · Jun Zhang[2] · Hong Quan[1] · Hao Peng[1]

Received: 26 December 2017 / Revised: 16 March 2018 / Accepted: 29 March 2018 / Published online: 9 October 2018

Abstract Nanoparticles (NPs) with high-*Z* atoms have been widely studied as radiosensitizers for use in cancer therapy. Over the past few years, the application of FePt NPs has attracted extensive research interest. Promising results have been obtained, yet limited knowledge is available regarding its potential use as a radiosensitizer. The goal of this study is to investigate the radiosensitization capability of FePt nanoparticle clusters (NPCs) under the exposure of kilovoltage photons using Monte Carlo simulation. First, in order to obtain a realistic distribution of NPCs on the microscopic level, Hela cells were incubated with FePt NPs, and the distribution of NPCs was obtained by optical microscope images and X-ray Nano-CT experiments. Based on these images, a simplified cell model was developed to evaluate the DER of two material types (FePt and $FePt_3$). For each type, the dependence of DER on the thickness and angular distribution of NPCs on the surface of the cell membrane was studied quantitatively. Our results suggest that DER is strongly dependent on photon energy and the distance from the NPCs to the nucleus. Fe_1Pt_3 is able to achieve a higher DER relative to Fe_1Pt_1. For a given X-ray energy, DER demonstrates an initial increase to a maximum value but gradually saturates as the thickness of NPCs increases from 250 up to 2000 nm due to a trapping effect. The impact on DER resulting from the coexistence of the NPCs on the cell membrane and the nuclear membrane was also investigated.

Keywords FePt nanoparticle · Radiosensitization · GEANT4 · Dose enhancement ratio

1 Introduction

Recently, high-Z nanoparticles (NPs) have been widely investigated in radiation therapy due to their roles in radiosensitization [1–4]. These nanoparticles can increase the photoelectric cross section of incident photons and consequently enhance the energy deposited in the vicinity of nanoparticles. In addition, through specific binding with chemical ligands, these NPs will preferentially accumulate in cancer cells while staying away from normal cells [5–7]. Gold nanoparticles (GNP) have been extensively studied due to their biocompatibility and high atomic number. The radiosensitization effect of GNPs on cancer cells or mice was investigated through both Monte Carlo simulations and in vitro studies [8, 9]. The detailed characteristics of secondary electrons generated by GNPs under X-ray

This study was supported by the Natural Science Foundation of China (Nos. 10875092 and 31271511), and the Natural Science Foundation of Hubei Province of China (No. 2012KB04449). The authors thank sincerely to the Department of Radio- and Chemo-therapy, Zhongnan Hospital of Wuhan University, Wuhan, China, and Elekta Instrument (Shanghai) Ltd., for providing the experimental environment for this research.

✉ Hong Quan
00007962@whu.edu.cn

✉ Hao Peng
00031619@whu.edu.cn

Zhi-Tao Dai
daizt_sinap@163.com

[1] Key Laboratory of Artificial Micro- and Nano-Structures of the Ministry of Education and Center for Electronic Microscopy and Department of Physics, Wuhan University, Wuhan 430072, China

[2] Department of Radiation Oncology, Zhongnan Hospital, Wuhan University, Wuhan 430072, China

irradiation were also studied [10]. Moreover, the dose enhancement ratio (DER) of GNPs under various conditions and geometries at the microscopic level was investigated [1].

As a novel nanomaterial, the potential use of FePt NPs exists in multiple fields, including diagnostic imaging (MRI and CT) and cancer therapy because of their structural stability, superparamagnetic property, and photothermal effect [11–13]. For example, FePt NPs have been successfully used in the field of magnetic resonance imaging as a contrast agent due to the presence of iron particles [14]. The use of FePt NPs as a radiosensitizer was first proposed in [14, 15]. The atomic number of Pt ($Z_{Pt} = 78$) is comparable to gold ($Z_{Au} = 79$), and therefore, similar dose enhancement is expected. In addition, it is well known that platinum-based chemotherapy drugs can bind to DNA and destroy its structure as a chemotherapy agent [16]. Thus, FePt NPs could also be used as chemotherapeutic drugs. When compared with traditional chemotherapy drugs, Pt-based nanoparticles are less likely to penetrate the tight junctions of the endothelial cells within normal blood vessels, thus resulting in low concentration in normal tissues [17, 18].

So far, NP clusters (NPCs) reported in cell cultures include ceramic oxide NPs, gold NPs [19], and FePt NPs [14, 15]. This work aims to evaluate the radiosensitization effect of FePt NPs for the first time. Experimental work in our group has investigated the promise of using FePt NPs as chemoradiotherapy sensitizers under irradiation with kilovoltage photons, in which a greater cellular suppression effect is observed [20]. Two similar studies investigated the radiosensitization of AuNPs in melanoma under irradiation with kilovoltage photons (150 keV) [21, 22]. The potential use of gadolinium NPs under 30–80 keV for both imaging and therapeutic enhancement agents was also reported recently [23].

In this study, we investigated the radiosensitization effect of FePt NPCs using the Geant4 Monte Carlo simulation (version Geant4.10.2.P02) [24]. First, cancer cells (H1975) were incubated with FePt NPs, and the distribution of NPs was derived from optical microscope images and X-ray Nano-CT experiments. Second, the simulation model was built based on the distribution in the first section, and DER was calculated under various conditions in terms of photon energy, thickness, and angular coverage of NPCs.

2 Materials and methods

2.1 Cell culture and characterization

Hela cell line (human cervical carcinoma cancer) was ordered from the Type Culture Collection of Chinese Academy of Sciences (Shanghai, China) and cultured in RPIM media with 10% fetal bovine serum, 100 U/mL penicillin, and 100 mg/mL streptomycin at 37 °C in a humidified incubator with 5% CO_2. Cells were seeded (3×10^5 per well) for cell attachment in 6 well plates for 24 h. The cells were then exposed to FePt NPs at 20 μg/mL for 24 h and washed twice with PBS afterward. The distribution of NPs was measured using an optical microscope.

X-ray Nano-CT imaging was performed to determine the distribution of NPCs around individual cells. 100-mesh TEM grids were used to carry the cells. Grids with the specimens were mounted in a homemade plunge freezer and were rapidly put into liquid nitrogen in a movable cryo-preserving container. The rapid plunge procedure was in place to avoid contamination by ice crystallization in order to protect the cells from structural damage. Grids with cells were then transferred into the soft X-ray imaging vacuum cryogenic chamber with a side-entry holder for imaging.

The X-ray Nano-CT experiment was performed with the BL07W beamline at the National Synchrotron Radiation Laboratory (Hefei, China). Selected quasi-monochromatic X-rays were focused by an elliptical capillary condenser. Coupled with a microzone plate, the system can perform imaging with X-ray energies between 280 and 700 eV (spatial resolution: 30 nm). In our study, the energy was set to 520 eV, and the exposure time for each projection was 1 s.

For illustration, the distribution profiles of the FePt NPs are shown in Fig. 1a. It can be seen that the NPs aggregate around the cells and indeed form irregular clusters. The image is also consistent with the transmission electron microscope (TEM) images in our previous study [15]. The CT images (Fig. 1b, c) reveal a more detailed structure of the NPCs around a single cell. The distribution of thicknesses of the formed clusters is measured using the CT images, as shown in Fig. 1d and the average thickness is found to be 700 nm.

2.2 Monte Carlo simulation

2.2.1 Monte Carlo set-up

The list of physics models and the transportation processes for photons and electrons is summarized in Table 1. Geant4-DNA extension was utilized to calculate the energy deposition in water [25, 26]. The Penelope Low Energy Package [27] was chosen to model the interactions inside the NPCs, since the Geant4-DNA is currently only available for simulation in liquid water. The G4 Urban model was used to model multiple scattering of electrons and ions. The threshold energy of electrons inside the NPCs was set to 100 eV, and the step cut was set to 1 nm. Atomic de-excitation, including fluorescence and Auger electron emission, was included in all simulations.

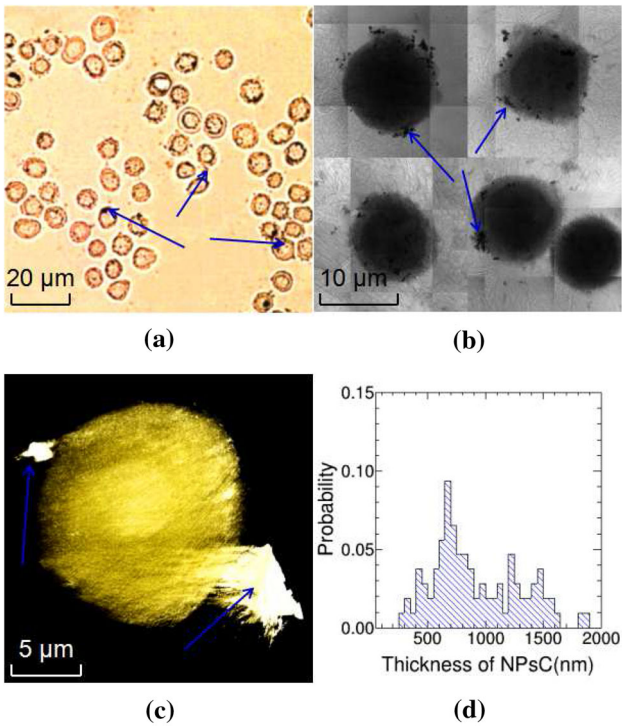

Fig. 1 (Color online) Images of cells labeled with FePt nanoparticles. **a** Optical microscopic image (the FePt nanoparticle cluster is indicated by arrows) and **b**, **c** soft X-ray images. Within a single cell, the FePt nanoparticle cluster is attached to the surface (represented by the structures of high brightness). **d** Cluster thickness distribution (mean value: $\sim$ 700 nm)

Table 1 Physical processes for photons and electrons in the NPCs and water

Particle	NPsC	Water
Photon	Rayleigh scattering[a]	Rayleigh scattering[a]
	Photoelectric effect[a]	Photoelectric effect[a]
	Compton scattering[a]	Compton scattering[a]
	Gamma conversion[a]	Gamma conversion[a]
Electron	Multiple scattering[a]	Elastic scattering[b]
	Ionisation[a]	Excitation[b]
	Bremsstrahlung[a]	Ionization[b]
		Vibrational excitation[b]

[a]G4_Penelope

[b]G4_DNA

Based on our previous work [15], two materials were investigated: $Fe_{26}Pt_{74}$ and $Fe_{53}Pt_{47}$ (the ratios of Fe:Pt were approximately 1:3 and 1:1), which have densities of 18.43 g/cm^3 and 15.12 g/cm^3, respectively. Note that the density of nanoparticle clusters is not equivalent to the density of the nanoparticles themselves. According to the work of Charles Kirkby et al. [28], we assume that FePt nanoparticles are tightly packed in a hexagonal geometry and the packing efficiency is roughly 74%. Therefore, the overall density of nanoparticle clusters could be defined as a mixture comprising 74% (volume fraction) FePt and 26% (volume fraction) water. As shown in Fig. 2, the X-ray spectrum selected in our study was 60 kVp, 150 kVp, and 200 kVp, based on previously published work [29].

2.2.2 *Cell models used in our simulations*

Based on the CT images, a cellular model with FePt NPCs was developed for simulation. A cell (the outer sphere) enclosing a nucleus (the inner sphere) was placed in liquid water, as shown in Fig. 3. θ_1 and θ_2 represent the angular coverage of the cluster over the surface of the cell and nucleus, respectively. d_1 is the distance between cluster and the center of nucleus. t_1 and t_2 represent the thickness of cluster found on the cell membrane and the nucleus membrane, respectively. The thickness of the nanoparticle cluster is defined as the geometric width of the cluster, as indicated by t_1 and t_2 in Fig. 3. This way, the overall effect of dose enhancement due to clustering on both the cell and nucleus can be evaluated simultaneously. For simplicity, the cell and nucleus were filled up with water. The incident beam of X-ray photons was simulated as a planar source (circular cross section) with radius r_1, and the distance between the source planar and the center of the cell was 10 μm. According to the distribution/size of the cell images in Fig. 1, the cell and nucleus radii were selected to be 5 μm and 2 μm, respectively. Radiosensitization was evaluated by calculating the dose enhancement ratio (DER), which is defined as follows:

$$\mathrm{DER} = \frac{D_{\mathrm{w}}}{D_{\mathrm{w/o}}}. \quad (1)$$

D_{w} and $D_{\mathrm{w/o}}$ are the dose deposition in the nucleus with and without NPCs, respectively. Since the therapeutic effect is primarily related to DNA damage, the dose exposure over the nucleus was used to calculate DER.

The simulation above was repeated for a set of scenarios. First, two kinds of NPCs ($FePt_3$ and FePt), three photon energies (60 kVp, 150 kVp, and 200 kVp), three distances between nucleus and cell ($d_1 = 3$ μm, 5 μm, and 7 μm), and three angular coverage cases ($\theta_1 = \pi/3, 2\pi/3, \pi$; $\theta_2 = 0$) were considered. Second, we investigated the radiosensitization effect when NPCs appears on the nuclear membrane and the cell membrane simultaneously. In this case, different NPC thicknesses on the cell membrane ($t_1 = 0$ nm, 250 nm, 750 nm, 500 nm, 1000 nm, and 1500 nm) were investigated when d_1 was selected to be 5 μm and θ_1, θ_2 were selected to be π. The thicknesses of NPCs on the surface of the nucleus was difficult to quantify based on CT images due to limited spatial resolution.

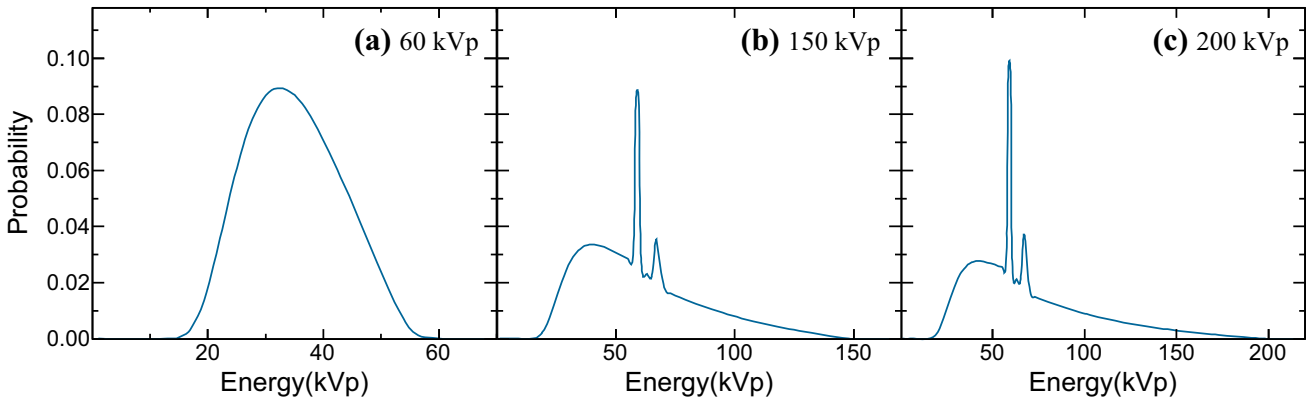

Fig. 2 Three energy spectra of the kV photons used in this simulation study. **a** 60 kVp, **b** 150 kVp and **c** 200 kVp

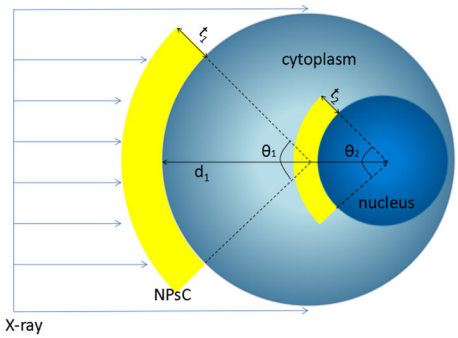

Fig. 3 (Color online) Schematic diagram of a simplified cell model used in this study (side view). t_1 and t_2 are the thickness of the cluster on the cell membrane and the nucleus membrane, respectively. d_1 is the distance between the cluster and the center of the nucleus. The NPCs are represented by the structures highlighted in yellow

Nevertheless, our previous TEM results suggest that the thickness is on the same order of magnitude as that on the cell membrane [15].

3 Results

3.1 Dependence of DER on material type, photon energy, and geometry

The results are shown in Fig. 4a. First, for each type of nanoparticle, DER demonstrates an initial increase up to a peak, followed by gradual saturation. The peak occurs around 800 nm for 60 kVp, while for 150 kVp and 200 kVp, saturation begins at 1400 nm. Second, a lower photon energy results in a higher DER value. For Fe_1Pt_3, the peak DER values are 42.58 (60 kVp), 26.96 (150 kVp), and 25.45 (200 kVp). This is expected, as the interaction probability between NPs and kV photons is inversely proportional to the photon energy. Third, compared to Fe_1Pt_1, $FePt_3$ NPCs induce a higher DER under a given energy. This can be attributed to the fact that the cross section of Pt is larger than that of Fe, thus making $FePt_3$ a more attractive radiosensitizer than Fe_1Pt_1. Such a comparison is also consistent with the experimental results [15], claiming Fe_1Pt_3 can cause a larger cell suppression ratio. This difference is more noticeable for the 60 kVp case. When t1 is 800 nm, DER is 38.97 (Fe_1Pt_1) and 42.58 (Fe_1Pt_3) (i.e., a difference of 9.2%).

The dependence of DER on the thicknesses d_1 and t_1 is shown in Fig. 4b, c, respectively. When t_1 is 1400 nm and the photon energy is 150 kVp, the DER value is 42.58 (3 μm), 26.96 (5 μm), and 16.41 (7 μm), respectively. In other words, greater DER values would occur when the NPCs are closer to the nucleus. This can be explained by the following process. Besides generating electrons with higher energies due to photoelectric or Compton interactions, most secondary electrons emitted are Auger electrons with lower energies and could only travel a limited distance. As d_1 increases, the number of Auger electrons that can reach the nuclear volume decreases, thus having limited contribution to energy deposition. On the other hand, the peak DER values (Fe_1Pt_3) are 12.31 ($1/3\pi$), 25.52 ($2/3\pi$), and 26.96 (π). This is due to the increased interaction probability between NPCs and photons as the surface area of NPCs increases.

3.2 Impact of NPsC on nuclear membrane and cell membrane

The results of DER for a set of t_1 and t_2 combinations are shown in Fig. 5. The DER value is larger compared to the results in Fig. 4. This is mainly because the NPCs are located on the surface of the nucleus, and those electrons generated are able to deposit most of their energy into nucleus, thus increasing DER.

Second, it is observed that when t_2 is 100 nm, a significant difference is observed among three t_1 values. DER is 27.95 (0 nm), 50.24 (500 nm), and 60.38 (1000 nm). However, when t_2 is 1000 nm, such a difference becomes

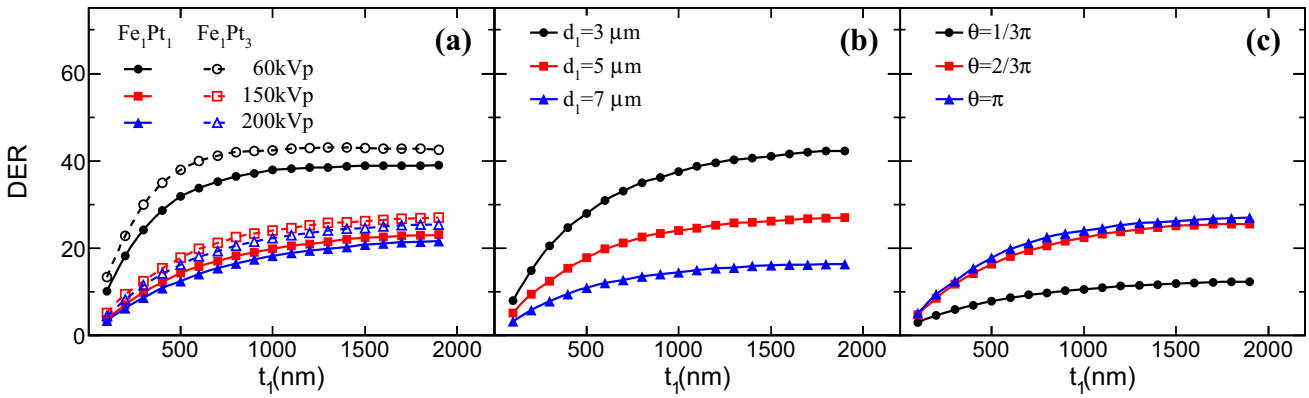

Fig. 4 (Color online) Dose enhancement ratio (DER) as function of t_1 for different scenarios. **a** DER dependence on material type and photon energy ($d_1 = 5\,\mu m$, $\theta = \pi$). **b** DER dependence on d_1 (energy: 150 kVp, Fe_1Pt_3, $\theta = \pi$). **c** DER dependence on θ (energy: 150 kVp, Fe_1Pt_3, $d_1 = 5\,\mu m$)

less noticeable. DER is 92.63 (0 nm), 93.96 (500 nm), and 98.21 (1000 nm). This implies that as the NPs start to accumulate on the surface of the nucleus, accumulation actually plays a crucial role in determining DER by excluding the dose exposure originating from NPCs on the cell membrane. In other words, DER is mutually dependent on both the cytomembrane cluster (NPCs on the cell membrane) and the karyotheca cluster (NPCs on the nuclear membrane). Secondary electrons emanating from these two clusters both contribute to the energy deposition over the nucleus. As the thickness of the karyotheca cluster increases above a certain threshold, electrons generated at the cytomembrane cluster may not be able to pass through the karyotheca cluster due to its short travel range in metal (i.e., electrons with energy less than 10 keV have a range of about 1 μm in FePt NPCs).

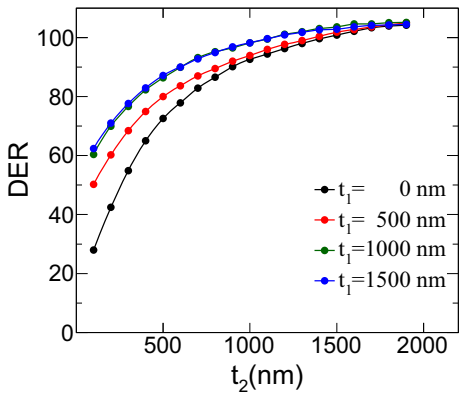

Fig. 5 (Color online) DER as a function of t_1 and t_2 due to the coexistence of clusters on the surface of the cell membrane and the nucleus

3.3 Behavior of secondary electrons

In this section, θ_1 was set to be π so that all the photons would travel through the nanoparticle clusters. The average number generated within NPCs and entering the cell is shown in Fig. 6a, b, respectively. It is observed that the number of electrons within the cluster increases linearly with the thickness of NPCs, while the number of electrons

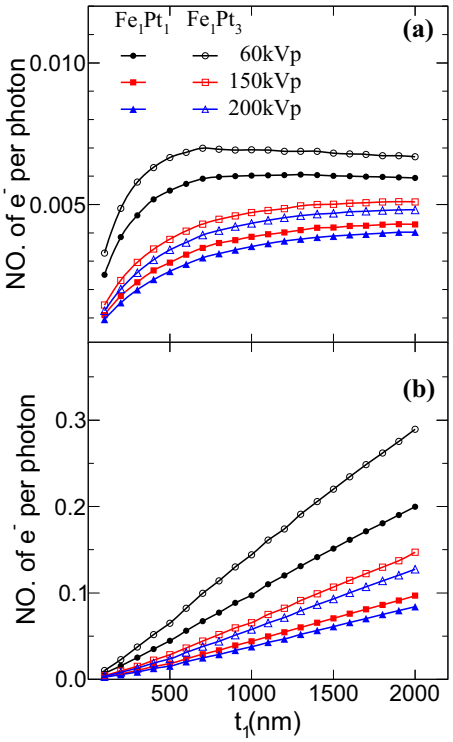

Fig. 6 (Color online) Yield of secondary electrons produced within NPCs for three photon energies and two material types. **a** The number of secondary electrons entering the cell. **b** The number of secondary electrons per incident photon

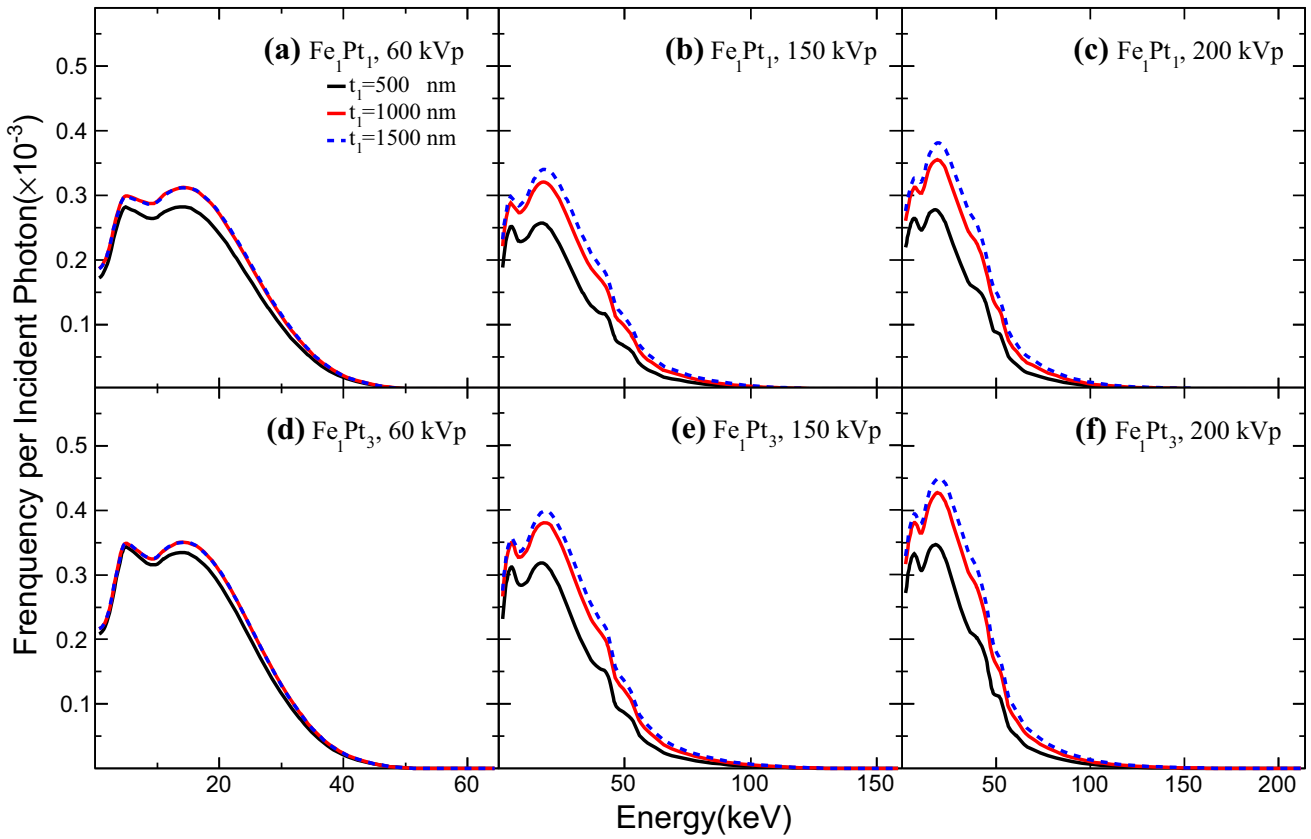

Fig. 7 (Color online) Normalized kinetic energy spectra (after normalization) of electrons entering the cell as a function of *t* under various conditions. **a** Fe_1Pt_1, 60 keV. **b** Fe_1Pt_1, 150 keV. **c** Fe_1Pt_1, 150 kVp. **d** Fe_1Pt_3, 60 keV. **e** Fe_1Pt_3, 150 keV. **f** Fe_1Pt_3, 150 kVp

entering the cell reaches a plateau after an initial increase. This trend is consistent with that shown in Fig. 4.

The kinetic energy spectra for those secondary electrons that are able to enter the cell are shown in Fig. 7. Besides several minor discrepancies observed in the low-energy region, the spectra of FePt and $FePt_3$ are very similar to each other. In addition, the relative yield of low-energy electrons (less than 10 keV) slightly decreases as the thickness of NPCs increases. This can be attributed to the fact that those electrons with kinetic energy less than 10 keV have an average range of less than 1 μm in NPCs. As the size of the cluster grows, they are more likely to be trapped inside and cannot escape to release their energies to the cell and the nucleus.

Such a trapping effect can be used to explain the dependence of DER on the thickness of the NPCs, as shown in Figs. 4a, 5 and 6a. While a larger cluster produces more electrons, a larger portion of them will be trapped inside at the same time. As a result, the number of electrons entering the cell/nucleus will not necessarily increase. The DER plateau occurs when the production and trapping of electrons compete against each other and eventually reach an equilibrium.

4 Discussion and conclusion

Our work aims to investigate the potential use of FePt NPs under the exposure of kilovoltage X-rays as motivated by a number of previous reports [14, 15, 20–23]. It should be pointed out that the kilovoltage X-rays are primarily used for treating tumors in skin or superficial tissues [30]. From the results in this paper, the potential use of FePt NPs as radiosensitizers under irradiation with kilovoltage photons may be useful for cancers within superficial tissues, such as melanoma.

The definition of DER is itself a challenging task and cannot be easily validated against experimental results. In our study, the quantitative DER results are derived based upon a simplified model (only a single cell was considered). Several additional factors need to be added into the model for further validation when compared to a realistic setting. For instance, either changing the size of source or using a cell matrix model will result in a lower DER value because those electrons produced in the surrounding medium after irradiation must now be taken into account, as well as the shielding effect due to the presence of adjacent cells. One primary challenge here relates to determining the spatial distribution of NP clusters in the

cell culture and the exact locations of NP clusters relative to the cell matrix. In terms of the shielding effect, this occurs only when photons travel across both the clusters located on the cell and nuclear membranes. In reality, however, the shape of clusters will be highly irregular and the shielding effect may be not as significant as the results in our study show. These limitations are beyond the scope of our current work and will be included in a future study.

Another practical consideration is the concentration of nanoparticles when being used as radiosensitizers. Increasing the concentration of nanoparticles would boost the growth of nanoparticle clusters, which subsequently increases the thickness of the cluster but does not necessarily promote its radiosensitization capacity [2]. Meanwhile, if the concentration becomes high, the number of nanoparticles entering into normal cells will also increase, resulting in undesired damage to normal tissue [14, 15]. On the other hand, experimental techniques also need to be improved to control the formation of NP super-clusters (i.e., hundreds of microns) during material synthesis. Besides its impact on DER, these super-clusters may also prevent the nanoparticles from entering into the tumor cell. For example, some surfactants (e.g., sodium dodecyl benzene sulfonate) could be attached to FePt nanoparticles to limit the effect of clustering.

In conclusion, our work investigated the radiosensitization effect of FePt NPCs for the first time. DER was studied using a model at the microscopic level with Monte Carlo simulation tools. The dependence of DER on a number of parameters was obtained, including photon energy, two material types, and the cluster thickness. We examined two important processes related to the coexistence of NPCs on the cell membrane and the nuclear membrane, and the resulting trapping effect for low-energy secondary electrons. This work lays the foundation for us to develop more advanced macroscopic models for quantitative DER studies.

References

1. P. Zygmanski, B. Liu, P. Tsiamas, Dependence of Monte Carlo microdosimetric computations on the simulation geometry of gold nanoparticles. Phys. Med. Biol. **58**, 7961 (2013). https://doi.org/10.1088/0031-9155/58/22/7961
2. S. McKinnon, E. Engels, M. Tehei, Study of the effect of ceramic Ta_2O_5 nanoparticle distribution on cellular dose enhancement in a kilovoltage photon field. Phys. Med. **32**, 1216–1224 (2016). https://doi.org/10.1016/j.ejmp.2016.09.006
3. J. Kwon, K. Sutherland, T. Hashimoto, Spatial distributions of dose enhancement around a gold nanoparticle at several depths of proton Bragg peak. Nucl. Instrum. Methods Phys. Res. Sect. B **384**, 113–120 (2016). https://doi.org/10.1016/j.nimb.2016.08.013
4. H.N. Tran, M. Karamitros, V.N. Ivanchenko, Geant4 Monte Carlo simulation of absorbed dose and radiolysis yields enhancement from a gold nanoparticle under MeV proton irradiation. Nucl. Instrum. Methods Phys. Res. Sect. B **375**, 126–139 (2016). https://doi.org/10.1016/j.nimb.2016.01.017
5. P.-C. Chiang, D.-S. Hung, J.-W. Wang, Engineering water-dispersible FePt nanoparticles for biomedical applications. IEEE Trans. Magn. **44**, 1768–1772 (2008). https://doi.org/10.1109/TMAG.2007.894341
6. R. Hong, N.O. Fischer, T. Emrick, Dependence of Monte Carlo microdosimetric computations on the simulation geometry of gold nanoparticles. Chem. Mater **17**, 4617–4621 (2005). https://doi.org/10.1021/cm0507819
7. N. Chattopadhyay, Z. Cai, J. Pignol, Design and characterization of HER-2-targeted gold nanoparticles for enhanced X-radiation treatment of locally advanced breast cancer. Mol. Pharm. **7**, 2194–2206 (2010). https://doi.org/10.1021/mp100207t
8. J.F. Hainfeld, D.N. Slatkin, H.M. Smilowitz, The use of gold nanoparticles to enhance radiotherapy in mice. Phys. Med. Biol. **49**, N309 (2004). https://doi.org/10.1088/0031-9155/49/18/N03
9. J.F. Hainfeld, F.A. Dilmanian, Z. Zhong, Gold nanoparticles enhance the radiation therapy of a murine squamous cell carcinoma. Phys. Med. Biol. **55**, 3045 (2010). https://doi.org/10.1088/0031-9155/55/11/004
10. M.K.K. Leung, J.C.L. Chow, B.D. Chithrani, Irradiation of gold nanoparticles by x-rays: Monte Carlo simulation of dose enhancements and the spatial properties of the secondary electrons production. Med. Phys. **38**, 624–631 (2011). https://doi.org/10.1118/1.3539623
11. S.-W. Chou, Y.-H. Shau, P.-C. Wu, In vitro and in vivo studies of FePt nanoparticles for dual modal CT/MRI molecular imaging. J. Am. Chem. Soc. **132**, 13270–13278 (2010). https://doi.org/10.1021/ja1035013
12. S. Sun, Recent advances in chemical synthesis, self-assembly, and applications of FePt nanoparticles. Adv. Mater. **18**(4), 393–403 (2006). https://doi.org/10.1002/adma.200501464
13. C.-L. Chen, L.-R. Kuo, S.-Y. Lee, Photothermal cancer therapy via femtosecond-laser-excited FePt nanoparticles. Biomaterials **34**, 1128–1134 (2013). https://doi.org/10.1016/j.biomaterials.2012.10.044
14. Y. Zheng, Y. Tang, Z. Bao, FePt nanoparticles as a potential X-ray activated chemotherapy agent for HeLa cells. Int. J. Nanomed. **10**, 6435–6444 (2015). https://doi.org/10.2147/IJN.S88458
15. Z. Bao, M. He, H. Quan, FePt nanoparticles: a novel nanoprobe for enhanced HeLa cells sensitivity to chemoradiotherapy. RSC Adv. **6**, 35124–35134 (2016). https://doi.org/10.1039/C6RA03990A
16. E. Porcel, S. Liehn, H. Remita, Platinum nanoparticles: a promising material for future cancer therapy? Nanotechnology **21**, 085103 (2010). https://doi.org/10.1088/0957-4484/21/8/085103
17. E. Porcel, S. Liehn, H. Remita, Platinum nanoparticles: a promising material for future cancer therapy? J. Am. Chem. Soc **131**(42), 15346–15351 (2009). https://doi.org/10.1021/ja905938a
18. Y. Zhang, W.-X. Yang, Tight junction between endothelial cells: the interaction between nanoparticles and blood vessels. Beilstein J. Nanotechnol. **7**, 675–684 (2016). https://doi.org/10.3762/bjnano.7.60
19. S.J. McMahon, W.B. Hyland, M.F. Muir, Nanodosimetric effects of gold nanoparticles in megavoltage radiation therapy. Radiother. Oncol. **100**(3), 412–416 (2011). https://doi.org/10.1016/j.radonc.2011.08.026
20. Y. Sun, H. Miao, S. Ma, FePt-Cys nanoparticles induce ROS-dependent cell toxicity, and enhance chemo-radiation sensitivity of NSCLC cells in vivo and in vitro. Cancer Lett. **418**, 27–40 (2018). https://doi.org/10.1016/j.canlet.2018.01.024

21. S.R. Kim, E.H. Kim, Feasibility study on the use of gold nanoparticles in fractionated kilovoltage X-ray treatment of melanoma. Int. J. Radiat. Biol. **94**(1), 8–16 (2018). https://doi.org/10.1080/09553002.2018.1393579
22. E. Porcel, S. Liehn, H. Remita, Gold nanoparticles as dose-enhancement agent for kilovoltage X-ray therapy of melanoma. Int. J. Radiat. Biol. **93**(5), 517–526 (2017). https://doi.org/10.1080/09553002.2017.1276309
23. Y. Zhang, W.-X. Yang, Comparison of gadolinium nanoparticles and molecular contrast agents for radiation therapy-enhancement. Med. Phys. **44**(11), 5949–5960 (2017). https://doi.org/10.1002/mp.12570
24. S. Agostinelli, J. Allison, K. Amako, Geant 4—a simulation toolkit. Nucl. Instrum. Methods Phys. Res. Sect. A **506**(3), 250–303 (2003). https://doi.org/10.1016/S0168-9002(03)01368-8
25. S. Incerti, A. Ivanchenko, M. Karamitros, Comparison of GEANT4 very low energy cross section models with experimental data in water. Med. Phys. **37**(9), 4692–4708 (2010). https://doi.org/10.1118/1.3476457
26. M.A. Bernal, M.C. Bordage, J.M.C. Brown, Track structure modeling in liquid water: a review of the Geant4-DNA very low energy extension of the Geant4 Monte Carlo simulation toolkit. Phys. Med. **31**(8), 861–874 (2015). https://doi.org/10.1016/j.ejmp.2015.10.087
27. J. Sempau, J.M. Fernández-Varea, E. Acosta, Experimental benchmarks of the Monte Carlo code penelope. Nucl. Instrum. Methods Phys. Res. Sect. B **207**(2), 107–123 (2003). https://doi.org/10.1016/S0168-583X(03)00453-1
28. J. Sempau, J.M. Fernández-Varea, E. Acosta, Dosimetric consequences of gold nanoparticle clustering during photon irradiation. Med. Phys. **44**(12), 6560–6569 (2017). https://doi.org/10.1002/mp.12620
29. W.B. Li, M. Mllner, M.B. Greiter, Monte Carlo simulations of dose enhancement around gold nanoparticles used as X-ray imaging contrast agents and radiosensitizers. Proc. SPIE **9033**, 90331K (2014). https://doi.org/10.1117/12.2043687
30. R. Hill, B. Healy, L. Holloway, Advances in kilovoltage x-ray beam dosimetry. Phys. Med. Biol. **59**, R183 (2014). https://doi.org/10.1088/0031-9155/59/6/R183